Optimizing Terahertz Communication Between Nanosensors in the Human Cardiovascular System and External Gateways

Jorge Torres Gómez, *Senior Member, IEEE*, Jennifer Simonjan, *Member, IEEE*,
Josep Miquel Jornet, *Senior Member, IEEE*, and Falko Dressler, *Fellow, IEEE*

Abstract—Nanotechnology enables the development of a new generation of devices at the scale of a few cubic micrometers that can sense, process, and communicate. Such small, imperceptible devices will revolutionize healthcare applications and enable new possibilities for in-body environments. This paper studies the intra-body communication channel between nanosensors flowing in the bloodstream and gateways attached to the skin using the terahertz (THz) spectrum. The channel model considers three layers through which the waveform travels: skin, tissue, and blood. To optimize the communication performance, this work investigates the impact of noise and mobility, and subsequently derives the trade-off between them. We illustrate the achievable bit error rate (BER) for THz intra-body channels considering communication through human tissue layers, including noise and random mobility of nanosensors in the blood system.

Index Terms—Intrabody terahertz communication, Bit error rate, Channel model, In-body nanosensors

I. INTRODUCTION

NOVEL nanomaterials such as graphene have made it possible to fabricate sensors in the scale of a few hundred cubic nanometers [1], [2]. Such small sensors are envisioned to be flowing in the human circulatory system (HCS) to sense the smallest changes in physical variables like pressure, temperature and concentration of biological molecules [3]. Doing so, nanosensors will enable the detection of diseases at a much earlier development stage compared to what is possible at the moment [4]. One reason for late diagnosis of diseases such as cancer is that current sensing technologies mostly rely on the detection of tumors, i.e., large numbers of cancerous cells, or high concentrations of cancer biomarkers utilized among cancerous cells to coordinate [5]. Cancer biomarkers are on the nanometric scale and can only be detected through sensors with extraordinarily high sensitivity, generally in the size of the biomolecules themselves [6].

As depicted in Fig. 1, hundreds of nanosensors are foreseen to flow in the HCS to sense for abnormalities. Upon detecting

Jorge Torres Gómez and Falko Dressler are with the School for Electrical Engineering and Computer Science, TU Berlin, Berlin, Germany, email: {torres-gomez, dressler}@ccs-labs.org.

Jennifer Simonjan is with Technology Innovation Institute, Masdar City, Abu Dhabi, UAE, e-mail: Jennifer.Simonjan@tii.ae.

Josep Miquel Jornet is with the Department of Electrical and Computer Engineering and the Institute for the Wireless Internet of Things, Northeastern University, Boston, USA (e-mail: jmjornet@northeastern.edu)
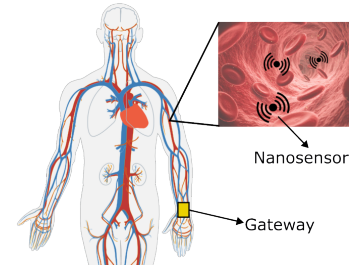
Fig. 1. Conceptual representation of nanosensors flowing through the HCS and a gateway attached to the hand of the person to collect the sensor data.

an abnormality, sensors should communicate their findings to the outside world. Collected sensor data can be transmitted to a gateway attached to the skin, making the data accessible to healthcare providers. A significant interest in this field is thus to develop communication strategies that enable sensors to send data through human tissue to the outside world. Such intra-body communication systems pose very difficult challenges, as nanosensors are highly resource-constrained and mobile, and human tissue causes significant path loss to electromagnetic communication rays.

Accounting for intra-body communication links, current literature suggests using the sub-terahertz (THz) band [7] as nanoscale graphene-based antennas can efficiently operate at the frequency range of 0.1–1 THz [8], [9]. Besides, from a communication theory perspective, attenuation and noise for intra-body links have been studied, providing accurate models to evaluate the signal to noise ratio (SNR) metric. Several works investigate the path loss of THz signals in blood and tissue, showing that communication in the range of a few millimeters is feasible [9]–[14]. Studies also introduce models for noise power in tissues, including the thermal noise at the receiver and the surrounding medium, as well as Doppler-shift-induced noise due to particle mobility in fluid mediums like the blood in the human vessels [15]. Modulation schemes have also been reported for improved reliability in such scenarios [16].

In this paper, we develop a transmission strategy to minimize the impact of noise and nanosensor mobility on the SNR. Although the impact of mobility is well understood in wireless [17] and ultrasound scenarios [18], there are no studies on the THz intra-body scenario. We propose to perform emissions along the channel coherence time while splitting data into packets. Furthermore, we evaluate the bit rate for the optimal balance between noise and nanosensor mobility

in human vessels. Increasing the bit rate reduces the impact of mobility by transmitting data with less variability in the nanosensor position but, at the same time, increases thermal noise by requiring more bandwidth. Thus, we identify a trade-off between noise and mobility in the transmission bandwidth.

To solve this trade-off, we provide an analytic formulation for the bit error rate (BER) following a similar methodology as in [17] for the wireless scenario. However, in our case we are taking into account the random mobility of nanosensors and the channel coherence time parameter in human vessels. According to this formulation, the best strategy is to transmit the data in a single packet (illustrated here with a packet size of $8\,\text{kB}$) when the nanosensor is located directly below the gateway and the transmission distance is the shortest.

II. System Model

Our proposed system comprises two different device types, the nanosensors which flow through the HCS and the gateways which are attached to the skin. The gateways are larger in scale, more powerful, and intended to collect the sensed data from the nanosensors as they flow by. Fig. 2 depicts our system model for the communication link, which assumes three layers of tissue comprising the blood vessel, the fat tissue and the skin. This means, nanosensors have to communicate their data through all three layers. To do so, they exploit sub-THz frequencies of 0.1–1 THz. To avoid communication at sites with too much attenuation, we assume that the gateway is placed on the skin surface at body sites where the veins are close below the skin (2–4 mm). Such body locations include, for example, wrists, hands, or ankles (where veins are directly visible).

We use the reference coordinate system outlined in Fig. 2 to describe the mobility of the nanosensors along the vessels. The origin of the coordinate system is located at the upper edge of the vessel, centered with the gateway (represented by $(0,0)$). Nanosensors flow in the veins horizontally, driven by the laminar flow of the blood [19]. Along the traveling direction, the x-position of the nanosensor is given by $x = v_{l_v}t$. The speed in the vertical direction v_{l_v} follows a parabolic profile as [20, Eq. (4.9) page 54]

$$v_{l_v} = \frac{4v_m}{L_v^2}(L_v l_v - l_v^2),\tag{1}$$

with maximum speed v_m and vessel thickness L_v. Along the vertical direction, the position of the nanosensor is random and uniformly distributed. This is in line with long observation times in fluids as motivated by the diffusion component of the nanosensor's mobility, see [21, Example 2]. Thus, we model l_v as uniformly distributed random variable of range $[0, l_v]$ with probability density function (PDF)

$$f_{l_v} = \frac{1}{L_v}.\tag{2}$$

III. Channel Model

As the nanosensors flow through the vessels passing by the gateway from left to right, the characteristics of the communication channel between the sensors and the gateway vary depending on the nanosensors' positions (see Fig. 3). We assume a communication scheme where nanosensors only
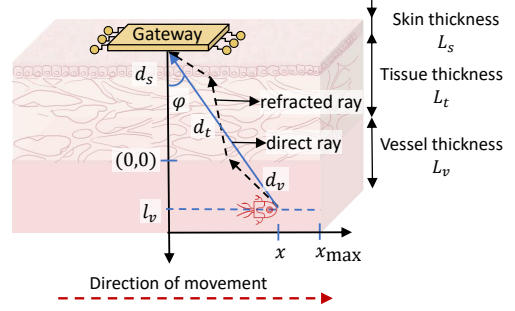
Fig. 2. Reference coordinate system for a nanosensor flowing through a blood vessel and communicating to a gateway outside the body.

send packets during the channel coherence time. The following subsections introduce channel path loss and coherence time as the two main channel parameters.

A. Channel Path Loss

The channel path loss depends on the thicknesses of the tissue layers through which the communication ray travels. According to Snell's law and as depicted in Fig. 2, the ray is refracted at each tissue boundary [22]. We model the vessel, tissue, and skin layer with thicknesses of L_v, L_t, and L_s, respectively. The path of the communication ray can be determined with Snell's law of refraction for boundaries between two mediums [23, Chap. 5 Eq. (5-15)]. At any boundary between two mediums (e.g., vessel to tissue or tissue to skin), the path of the refracted ray is determined by the respective refraction angle. Exploiting Snell's law, we can determine the exact traveling path of the communication ray from the nanosensor to the gateway. The refraction angles are evaluated according to the relation

$$\beta_i \sin\varphi_i = \beta_r \sin\varphi_r,\tag{3}$$

where φ_i and φ_r are the incident and refracted angles, and β_i and β_r are the phase constant coefficients of medium i and medium r, respectively. The phase constant β_i is computed as $\beta_i = \text{Im}(\delta_i)$, whereby δ_i is the propagation constant and is defined according to [23, Eq. (3-17c)] as

$$\delta_i^2 = j\omega\mu_i\sigma_i - \omega^2\mu_i\epsilon_i,\tag{4}$$

where $\mu_i = 1$ is the permeability [9], σ_i is the conductivity, and ϵ_i the permittivity. The parameter β_r for the refracted medium is evaluated similarly to β_i. The computation of the phase constant coefficients for all mediums showed that the refracted angle is approximately equal to the incident angle as

$$\frac{\beta\text{v}}{\beta\text{t}} = 0.924 \approx 1 \quad\text{and}\quad \frac{\beta\text{t}}{\beta\text{s}} = 1.153 \approx 1.$$

Thus, we can estimate the refracted ray path as the direct path between the nanosensor and the gateway (blue arrow in Fig. 2).

The path loss depends on the x-position of the nanosensor and the angle of incidence (φ in Fig. 2) at the gateway. The actual path lengths of the ray in each tissue can be evaluated using trigonometric functions as

$$d_v = \frac{L_v}{\cos\varphi} \quad, \quad d_t = \frac{L_t}{\cos\varphi} \quad\text{and}\quad d_s = \frac{L_s}{\cos\varphi},\tag{5}$$

$$\text{with}\quad \cos\varphi = \sqrt{1 - \left(\frac{v_{l_v}t}{l_v + L_t + L_s}\right)^2},$$
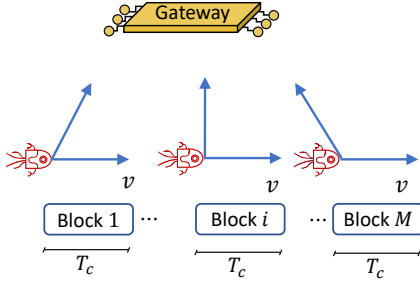
Fig. 3. Transmission blocks of the length of the coherence time transmitted at different positions.

where v_{l_v} is the nanosensor speed along the vertical direction as given in Eq. (1). The evaluation of $\cos\varphi$ assumes that transmissions start at $t = 0$ and $\varphi = \frac{\pi}{2}$ (just below the gateway, with the shortest distance and lowest attenuation). As each medium causes different path loss characteristics, the total path loss is a product of the medium-specific path losses as [14]

$$P_{\mathrm{L}} = e^{-\mu_v d_v} \times \left(\frac{\lambda_v}{4\pi d_v}\right)^2 \times e^{-\mu_t d_t} \times \left(\frac{\lambda_t}{4\pi d_t}\right)^2 \\ \times e^{-\mu_v d_s} \times \left(\frac{\lambda_s}{4\pi d_s}\right)^2, \quad (6)$$

where μ_v, μ_t, μ_s are the molecular absorption coefficients, and λ_v, λ_t, and λ_s are the effective wavelengths of the vessel, tissue, and skin, respectively. To compute the molecular absorption coefficients and the effective wavelength, refer to [9, Eq. (10) and content below Eq. (2)].

B. Channel Coherence Time

We perform transmissions along time intervals as the channel coherence time. When transmitting within this time window the impact of mobility diminishes as the Doppler effect is negligible. Consequently, we split the data sequence into blocks of the same duration as the coherence time (see Fig. 3). For the coherence time, we follow the expression [24, Eq. 4.40.c]

$$T_c = \sqrt{\frac{9}{16\pi}}\frac{1}{\nu_{\max}}, \quad (7)$$

where $\nu_{\max} = v\frac{f_c}{c}$ is the maximum Doppler shift, v is the transmission speed, f_c is the center frequency, and c is the speed of light. Transmitting within this time interval avoids induced phase shifts on the received signal which would cause distortions [1]. For instance, if the transmitter uses phase shift keying (PSK) modulation, emitting symbols along the channel coherence time avoids a rotation of the received constellation points.

Assuming a SNR threshold γ_0 for error-free detection, bits must be transmitted at a rate of $(\mathrm{BW}\log(1 + \gamma_0))$, where BW refers to the channel bandwidth. The time duration of the complete sequence then results in $\frac{\text{packet size}}{\mathrm{BW}\log(1+\gamma_0)}$. Consequently, the complete sequence is split into M blocks given as

$$M = \left\lfloor \frac{1}{T_c}\frac{\text{packet size}}{\mathrm{BW}\log(1 + \gamma_0)} \right\rfloor. \quad (8)$$

---

[1] Transmissions in blocks increases overhead due to the insertion of preamble sequences per block (not analyzed in this contribution).

TABLE I
SIMULATION PARAMETERS

Parameter	Variable	Value	Reference
Center Frequency	f_c	0.5 THz	
Modulation Scheme	BPSK		
SNR threshold	γ_0	15 dB	
Packet size	packetsize	8 kB	
Pulse transmission energy [3]	E_{Tx}	5 mJ	
Blood speed in the veins	v	0.03 m/s	[19]
Skin thickness	L_s	86 μm	[11]
Tissue thickness	L_t	1.44 mm	[26]
Vessel thickness	L_v	477 μm	[27]

To illustrate the impact of the channel coherence time in transmissions, we consider the parameters in Table I. According to Eq. (8) and assuming $\mathrm{BW} = 3\,\mathrm{GHz}$, $\gamma_0 = 15\,\mathrm{dB}$ [2], $T_c = 8.3\,\mathrm{ms}$, and a packet size of $8\,\mathrm{kB}$, the resulting total of blocks is $M = 2$. This corresponds to performing two emissions in blocks of $4\,\mathrm{kB}$. This example illustrates that even a relatively low transmitter speed v results in a short coherence time, as small packets can not be transmitted in a single emission. The short channel coherence time is mainly due to the high center frequency f_c used in the THz band.

IV. FORMULATING THE COMMUNICATION PERFORMANCE

We formulate the communication performance by providing a closed-form expression for the BER. To provide such an expression, we first evaluate the SNR at the receiver (see Section IV-A) and account for the randomness of the nanosensor's position in the vessel. Then, we evaluate the outage probability per block to evaluate the BER in Section IV-B.

A. Instantaneous and Average SNR

The experienced SNR depends on the nanosensor location, which is defined by two coordinates, one in the horizontal and one in the vertical direction (see Fig. 2) given as

$$\gamma_{\mathrm{m}}(l_v) = \frac{P_{\mathrm{Tx}}}{N P_{\mathrm{L,m}}(l_v)}. \quad (9)$$

In this equation, $\gamma_{\mathrm{m}}(l_v)$ depends only on the vertical position of the nanosensor. The horizontal position increases according to the blood speed, as given by $v_{l_v}t$ in Eq. (5). The index $\mathrm{m} \in \{1, M\}$ denotes the specific block, and N the noise power [28, Eq. (3)]

$$N = 4k_{\mathrm{B}}T_{\mathrm{noise}}\mathrm{BW}, \quad (10)$$

with Boltzmann constant k_{B}, reference temperature $T_{\mathrm{noise}} = T_{\mathrm{rx}} + T_{\mathrm{mol}}$, receiver temperature T_{rx} and molecular absorption temperature T_{mol} [4]. As l_v is a random variable (see

---

[2] We assume this SNR as the resulting BER is less than 1×10^{-12} for binary phase shift keying (BPSK) transmissions, see [25]. This value enables us to neglect the impact of noise and evaluate the impact of mobility only.

[3] The energy is computed as $P_{\mathrm{Tx}}/\mathrm{BW}$ assuming a peak power amplitude of $P_{\mathrm{Tx}} = 5\,\mathrm{kW}$ [14] and a minimum transmission rate of 1 GHz.

[4] We assume a constant molecular absorption temperature for distances larger than $0.8\,\mathrm{mm}$, see [28, Fig. 8]. Assuming the standard case of constant receiver temperature, both assumptions yield a constant noise power in Eq. (10).

Eq. (2)), the resulting SNR in Eq. (9) will also be a random variable with PDF [29, Eq. (5-5)]

$$f_{\gamma_{\mathrm{m}}} = -f_{l_v} \left. \frac{dl_v}{d\gamma_{\mathrm{m}}} \right|_{l_v = \gamma_{\mathrm{m}}^{-1}(l_v)}, \tag{11}$$

where the minus sign is due to the monotonically decreasing dependence of γ_{m} on l_v. This relation equates the PDF of the two random variables γ_{m} and l_v, which are related through a decreasing monotonic function, as given in Eq. (9). Although a given closed-form expression can be obtained for the derivative term in Eq. (11), numerical methods are required to find the inverse relation of γ_{m} with l_v using Eq. (9).

B. Outage Probability and BER

The outage probability is the probability that the received SNR (γ_{m}) becomes less than the SNR threshold γ_0, therefore producing errors. Analytically, the outage probability is formulated as the probability that the received packet's SNR (γ_{m}) becomes less than a predefined threshold (γ_0)

$$p_{\mathrm{out,m}} = P[\gamma_{\mathrm{m}} < \gamma_0] = \int_0^{\gamma_0} f_{\gamma_{\mathrm{m}}} d\gamma_{\mathrm{m}}, \tag{12}$$

where the integral is evaluated using (11) as follows

$$p_{\mathrm{out,m}} = \int_{\gamma_{0,\mathrm{m}}^{-1}(l_v)}^{L_v} f_{l_v} dl_v = 1 - \frac{\gamma_{0,\mathrm{m}}^{-1}(l_v)}{L_v}, \tag{13}$$

and $\gamma_{0,\mathrm{m}}^{-1}(l_v)$ refers to the inverse relation of γ_{m} with l_v when equating $\gamma_0 = \gamma_{\mathrm{m}}$ in Eq. (9). This inverse relation needs to be solved numerically for l_v when $\gamma_{\mathrm{m}}(l_v) = \gamma_0$. Using the outage probability for a block m, it is also possible to evaluate the bit error probability for the given block as $p_{b,\mathrm{m}} = \frac{p_{\mathrm{out,m}}}{B_{\mathrm{m}}}$, where B_{m} refers to the total of bits per block. Then, the resulting BER is directly given as

$$\mathrm{BER} = 1 - \Pi_{\mathrm{m}=1}^{M} \left(1 - \frac{p_{\mathrm{out,m}}}{B_{\mathrm{m}}}\right). \tag{14}$$

This enables us to evaluate the BER of the transmission bandwidth for a given SNR threshold. The BW eventually defines the total of transmission blocks M with Eq. (8), and the perceived SNR level with Equations (9) and (10) to evaluate the resulting outage probability. When considering its dependency on the bandwidth, we can identify the trade-off between noise and the impact of mobility as detailed in the following section.

V. OPTIMIZING THE COMMUNICATION PERFORMANCE

When performing transmissions there is a trade-off between the impact of noise and mobility. Transmitting all data in a single block opportunistically just below the gateway (see Fig. 3) implies the least attenuation but the highest noise level due to the need for an increased bit rate and, thus, bandwidth. For instance, transmitting $8\,\mathrm{kB}$ in a single block requires a bandwidth of BW $\approx 5\,\mathrm{GHz}$ according to Eq. (8), and assuming $\gamma_0 = 15\,\mathrm{dB}$ and $T_c = 8.3\,\mathrm{ms}$ (see Section III-B). This results in a BER $\approx 6.5 \times 10^{-6}$ when the nanosensor is at the shortest distance to the gateway as $L_t + L_s \approx 1.44\,\mathrm{mm}$ (see Table I).

However, reducing the bit rate, and thus the transmission bandwidth, produces transmissions with increased path loss,
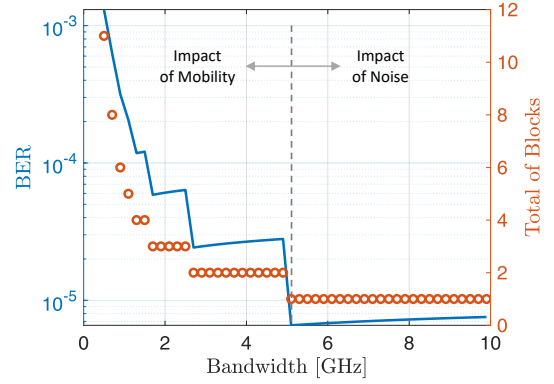
Fig. 4. Resulting BER and total of blocks M considering the parameters in Table I.

hence degraded performance (assuming a single gateway device as receiver). Due to a decreased transmission rate, the amount of data must be transmitted in multiple blocks. Consequently, the noise level is less (due to reduced bandwidth), but the attenuation increases (due to the moving nanosensor), which eventually degrades performance. This data partition process leads to a trade-off between noise and mobility.

In general, dividing the packet into M blocks depends on the outage probability per block as $p_{\mathrm{out,m}}$ in Eq. (13). Increasing the bit rate increases the bits per block, as BW increases (Eq. (8)). At the same time, the noise level increases (Eq. (10)), leading to an increased outage probability. Reducing the bit rate reduces noise, but requires transmissions more distant from the gateway as the nanosensor displaces(larger d_v, d_t, and d_s in Eq. (6)). This leads to an increased path loss, which reduces the perceived SNR, thereby increasing the outage probability.

Finding the transmission bandwidth that minimizes the BER in Eq. (14) must be solved numerically due to the lack of a closed-form expression for the inverse relation of the distance with the SNR per block as $\gamma_{0,\mathrm{m}}^{-1}(l_v)$ in Eq. (13). This is due to the exponential relationship of the path loss and the distances.

To solve this trade-off numerically, we use the function vpasolve in Matlab, which implements a Newton root search algorithm [5]. The results in Fig. 4 show the variability of the BER with the bandwidth and with the total of blocks, given the parameters in Table I. The minimum BER is experienced at a bandwidth of approx. $5\,\mathrm{GHz}$; which is achieved when performing transmissions in a single block.

Around this minimum, we can perceive the impact of mobility to the left and noise to the right. As the bandwidth becomes less, the total of blocks for transmission increases from 1 to 11, and consequently, the BER increases from 10^{-5} to 10^{-3} due to the increased path loss. To the right of the minimum, all transmissions are made in a single block with the same path loss, but increasing noise eventually degrades the BER as transmission bandwidth increases.

The location of the minimum BER varies depending on the physiological parameters of the vessels, however, the BER curve shows the same behavior. The BER increases with the thickness of the skin, tissue, or vessel. As the received
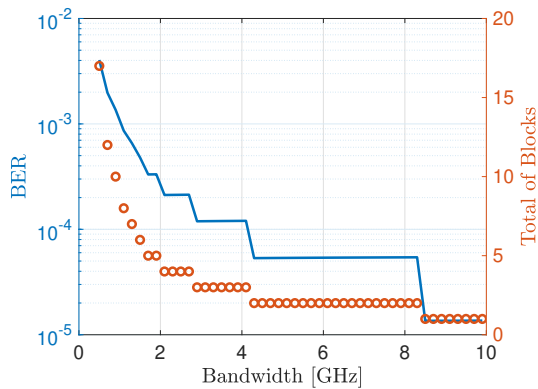
Fig. 5. Resulting BER and total of blocks M with parameters in Table I and increased vessel thickness and higher blood speed.

power decreases with the thickness of the tissues (see the inverse dependency of the power level P_{L} with thickness in Equations (5) and (6)), the SNR decreases, and thus, the outage probability and the BER increase. Besides, the minimum BER shifts to the right with increased blood speed. Higher blood speed shortens the channel coherence time and expands the transmission bandwidth to perform emissions in a single block. To illustrate, Fig. 5 depicts the results for an increased vessel thickness of $L_{\mathrm{vessel}} = 800\,\mu\mathrm{m}$ and higher blood speed of $v = 0.05\,\mathrm{m/s}$. Compared to Fig. 4, the minimum BER shifts above $8\,\mathrm{GHz}$ and is larger than $1{\times}10^{-5}$.

VI. CONCLUSIONS

This paper discussed an analytic model to evaluate the trade-off between noise and mobility for in-body to out-body communication links. The trade-off is stated to minimize the BER accounting for the random mobility of nanosensors, as passively guided by the blood flow, and noise and path loss along the human tissues in the THz band. When performing transmissions along the channel coherence time, results suggest that transmitting in a single block is the best strategy to minimize the impact of noise and mobility on the BER.

REFERENCES

[1] N. Panwar, A. M. Soehartono, K. K. Chan, et al., "Nanocarbons for Biology and Medicine: Sensing, Imaging, and Drug Delivery," *Chemical Reviews*, vol. 119, no. 16, pp. 9559–9656, Jul. 2019.

[2] J. Simonjan, J. M. Jornet, I. F. Akyildiz, and B. Rinner, "Nano-cameras: a key enabling technology for the internet of multimedia nano-things," in *ACM NANOCOM*, Reykjavík, Iceland: ACM, Sep. 2018.

[3] T. Nakano et al., "Methods and Applications of Mobile Molecular Communication," *Proceedings of the IEEE*, vol. 107, no. 7, pp. 1442–1456, Jul. 2019.

[4] T. Khan et al., "Nanosensor networks for smart health care," in *Nanosensors for Smart Cities*, Elsevier, 2020, pp. 387–403.

[5] M. Sitti, H. Ceylan, W. Hu, et al., "Biomedical Applications of Untethered Mobile Milli/Microrobots," *Proceedings of the IEEE*, vol. 103, no. 2, pp. 205–224, Feb. 2015.

[6] R. Mosayebi et al., "Early Cancer Detection in Blood Vessels Using Mobile Nanosensors," *IEEE Transactions on NanoBioscience*, vol. 18, no. 4, pp. 103–116, Oct. 2019.

[7] F. Lemic, S. Abadal, W. Tavernier, et al., "Survey on Terahertz Nanocommunication and Networking: A Top-Down Perspective," *IEEE Journal on Selected Areas in Communications*, vol. 39, no. 6, pp. 1506–1543, Jun. 2021.

[8] J. M. Jornet and I. F. Akyildiz, "Femtosecond-Long Pulse-Based Modulation for Terahertz Band Communication in Nanonetworks," *IEEE Transactions on Communications*, vol. 62, no. 5, pp. 1742–1754, May 2014.

[9] H. Elayan, R. M. Shubair, J. M. Jornet, and P. Johari, "Terahertz Channel Model and Link Budget Analysis for Intrabody Nanoscale Communication," *IEEE Transactions on NanoBioscience*, vol. 16, no. 4, pp. 491–503, Jun. 2017.

[10] I. F. Akyildiz et al., "Terahertz Band Communication: An Old Problem Revisited and Research Directions for the Next Decade," *IEEE Transactions on Communications*, vol. 70, no. 6, pp. 4250–4285, Jun. 2022.

[11] G. Piro et al., "Terahertz electromagnetic field propagation in human tissues: A study on communication capabilities," *Nano Communication Networks*, vol. 10, pp. 51–59, Dec. 2016.

[12] I. T. Javed, K. N. Qureshi, F. Alharbi, and G. Jeon, "Terahertz fading model for wireless nanosensor networks in advanced medical manufacturing technologies," *The International Journal of Advanced Manufacturing Technology*, Jul. 2022.

[13] N. Saeed et al., "Body-Centric Terahertz Networks: Prospects and Challenges," *IEEE Transactions on Molecular, Biological and Multi-Scale Communications*, vol. 8, no. 3, pp. 138–157, Sep. 2022.

[14] J. Simonjan, B. D. Unluturk, and I. F. Akyildiz, "In-body bionanosensor localization for anomaly detection via inertial positioning and THz backscattering communication," *IEEE Transactions on NanoBioscience*, vol. 21, no. 2, pp. 216–225, 2021.

[15] H. Elayan, C. Stefanini, R. M. Shubair, and J. M. Jornet, "End-to-End Noise Model for Intra-Body Terahertz Nanoscale Communication," *IEEE Transactions on NanoBioscience*, vol. 17, no. 4, pp. 464–473, Oct. 2018.

[16] S. Nagaraj and R. Yaqo, "A Frequency Modulation Technique for SNR Improvement in Backscatter Radios," *IEEE Communications Letters*, vol. 25, no. 12, pp. 3956–3959, Dec. 2021.

[17] A. Zaalouk, C. Mukasa, and G. P. Efthymoglou, "Effect of Mobility on the Outage and BER Performances of Digital Transmissions over Nakagami- Fading Channels," *IEEE Transactions on Vehicular Technology*, vol. 65, no. 2, pp. 2715–2721, Feb. 2015.

[18] J. T. Gómez, A. Kuestner, L. Stratmann, and F. Dressler, "Modeling Ultrasonic Channels with Mobility for Gateway to In-Body Nanocommunication," in *IEEE GLOBECOM*, IEEE, 2022, pp. 4535–4540.

[19] A. C. Guyton and M. E. Hall, *Guyton and Hall Textbook of Medical Physiology*, 14th ed. Elsevier, 2015.

[20] H. C. Berg, *Random Walks in Biology*. Princeton University Press, 1993.

[21] V. Jamali, A. Ahmadzadeh, W. Wicke, A. Noel, and R. Schober, "Channel Modeling for Diffusive Molecular Communication - A Tutorial Review," *Proceedings of the IEEE*, vol. 107, no. 7, pp. 1256–1301, Jul. 2019.

[22] H. Elayan, R. M. Shubair, J. M. Jornet, and R. Mittra, "Multi-layer Intrabody Terahertz Wave Propagation Model for Nanobiosensing Applications," *Elsevier Nano Communication Networks*, vol. 14, pp. 9–15, Dec. 2017.

[23] C. Balanis, *Advanced Engineering Electromagnetics*, 2nd ed. Wiley, 2012, p. 1040.

[24] T. S. Rappaport, *Wireless Communications: Principles and Practice*, 2nd ed. Upper Saddle River, NJ: Prentice Hall, 2009.

[25] A. B. Carlson, P. B. Crilly, and J. C. Rutledge, *Communication Systems: An Introduction to Signals and Noise in Electrical Communication*, 4th ed. New York City, NY: McGraw-Hill, 2002, p. 850.

[26] P. Oltulu et al., "Measurement of epidermis, dermis, and total skin thicknesses from six different body regions with a new ethical histometric technique," *Turkish Journal of Plastic Surgery*, vol. 26, no. 2, p. 56, 2018.

[27] M. Fruchard, L. Arcese, and E. Courtial, "Estimation of the Blood Velocity for Nanorobotics," *IEEE Transactions on Robotics and Automation*, vol. 30, no. 1, pp. 93–102, Feb. 2014.

[28] K. Yang et al., "Numerical Analysis and Characterization of THz Propagation Channel for Body-Centric Nano-Communications," *IEEE Transactions on Terahertz Science and Technology*, vol. 5, no. 3, pp. 419–426, May 2015.

[29] A. Papoulis, *Probability, Random Variables and Stochastic Processes*, 3rd ed. Boston, Mass.: McGraw Hill, 1991, p. 661.